

Supporting Information

for *Adv. Funct. Mater.*, DOI: 10.1002/adfm.202203064

Excellent Long-Range Charge-Carrier Mobility in 2D
Perovskites

Manuel Kober-Czerny, Silvia Genaro Motti, Philippe Holzhey, Bernard Wenger, Jongchul Lim, Laura Maria Herz,* and Henry James Snaith**

Supporting Information

Excellent long-range charge-carrier mobility in 2D perovskites

Manuel Kober-Czerny, Silvia Genaro Motti, Philippe Holzhey, Bernard Wenger, Jongchul Lim, Laura Maria Herz*, Henry James Snaith**

SI. 1 Optoelectronic Methods*UV-Vis*

Transmission and reflection spectra were measured for thin-film samples on microscope glass slides with a PerkinElmer 1050+ UV-Vis-NIR spectrophotometer equipped with an integrating sphere accessory. During the measurement both the sample and reference beam were attenuated to 1% to allow for better quality data of the excitonic feature with high optical density. This approach does not change the absorption spectrum measured. The absorption coefficient was calculated as

$$\alpha = \frac{1}{t} \cdot \ln\left(\frac{1-R}{T}\right) \quad (\text{S1})$$

where t is the thickness as measured with a DekTak Profilometer of the thin-film and R and T are the reflectance and transmission, respectively.

Transient Photo-Conductivity (TPC)

Using a home-built setup, the transient photoconductivity (TPC) was measured for the thin-films on glass.^[S1] Interdigitated gold electrodes spaced 300 μm apart were used to establish a weak electric field of $\leq 0.01 \text{ V } \mu\text{m}^{-1}$ (about 100 x lower than under standard solar cell operation). The sample was illuminated by a 10 Hz pulsed laser at 470 nm with power densities $< 1 \text{ mW cm}^{-2}$ (see **Table S2** for all the settings).

The same setup was used to measure the PL_0 values shown in **Figure S3** using a monochromator and a PMT detector.

Terahertz Spectroscopy (OTTP)

Optical-Pump THz-Probe experiments were performed as previously described.^[S2,S3] A Spectra Physics Mai Tai-Empower-Spitfire Pro Ti:Sapphire regenerative amplifier provides 35 fs pulses centered at 800 nm at a repetition rate of 5 kHz. 400 nm (3.10 eV) photoexcitation is obtained by frequency doubling the fundamental laser output through a BBO crystal, and 520 nm (2.38 eV) photoexcitation is obtained using an Optical Parametric Amplifier (Spectra Physics TOPAS). THz probe pulses are generated by a spintronic emitter composed of 1.8nm of $\text{Co}_{40}\text{Fe}_{40}\text{B}_{20}$ sandwiched between 2 nm of Tungsten and 2 nm of Platinum, all supported by a quartz substrate. Detection of the THz pulses was performed using electro-optic sampling in a ZnTe crystal (1 mm (110)-ZnTe). The samples studied were bare perovskite films deposited on z-cut quartz. The sample, THz emitter and THz detector were held under vacuum ($< 10^{-2}$ mbar) during the measurements.

Time-Resolved Photoluminescence (TRPL)

The photoluminescence decay curves were acquired on a FluoTime 300 (PicoQuant GmbH) using a TimeHarp 260 as time-correlated single photon counting setup (TCSPC) and a pulsed laser diode with an excitation wavelength of 405 nm (LHD-P-C-405, PicoQuant GmbH). The repetition rate of the diode was 0.5 MHz.

Photoluminescence Quantum Efficiency (PLQE)

Photoluminescence quantum efficiency measurements were carried out using a 405 nm laser (Roithner laser MLL-III-405-200 mW; for PEA_2PbI_4 samples), a 532 nm laser (Roithner laser RTLMLL-532-1.5-3W; for $\text{FA}_{0.9}\text{Cs}_{0.1}\text{PbI}_3$ samples), an integrating sphere, and a calibrated grating spectrometer (QEPro, OceanInsight), using previously established protocols.^[S4]

SI.2 Structural Characterization

Powder XRD

The XRD patterns were measured from the thin-films deposited on glass directly using a $\text{Cu K}\alpha$ X-Ray source and a X'PERT Pro Xray diffractometer (Panalytical). All samples were measured on z-cut quartz substrates.

2D XRD

2D XRD measurements were conducted in ambient air (30 to 50% RH) at room temperature using a Rigaku SmartLab X-ray diffractometer with a $\text{CuK}\alpha 1$ and a HyPix-3000 2D hybrid pixel array detector.

SEM

The SEM images of the thin films on glass were taken using a FEI Quanta 600 FEG scanning electron microscope. The thin films were deposited on indium tin oxide (ITO)-coated glass to allow for better image quality.

SI.3 Elliott Fit of 2D PEA₂PbI₄

A common approach to find the exciton binding energy is to fit the absorption coefficient according to Elliot's Theory.^[S5] In short, the absorption onset of a direct bandgap semiconductor can be described by a continuum of states modulated by the existence of sub-bandgap excitonic states.

It has been shown previously that Elliott's model cannot perfectly capture the absorption spectrum of metal halide perovskites, due to a strong Coulomb interaction within the material.^[S6] Only the first few hundred meV above the absorption can be fitted properly. Even though, a few hundred meV are enough for the purpose of this study to determine the difference in energy between the exciton and the continuum of states - the exciton binding energy E_B .

In addition to the strong Coulomb interactions, two-dimensional perovskites also show increased dielectric confinement, which influences the absorption properties. For this study a fitting procedure similar to the one described by J.V. Passarelli *et. al.* was used.^[S7] In short, the absorption coefficient α as obtained by **Equation S1** is fitted by an excitonic part α_{ex} and a continuum part α_c (see **Equation S2-S4**).

$$\alpha(E) = A \cdot (\alpha_{ex}(E) + \alpha_c(E)) \quad (\text{S2})$$

where A is an instrument-specific enhancement factor.

For the excitonic part, a series of normalized gaussian peaks with peak centre $E_g - E_B$ and broadening σ_{ex} are used. They are spaced in energy by E_{xm} . Special attention is given to the first excitonic peak (1s), which is best fitted by an asymmetric peak shape in case of the 2D PEA₂PbI₄. For that purpose, two different broadening terms $\sigma_{ex,1}$ and $\sigma_{ex,2}$ are used for each side of the peak, whereby $\sigma_{ex,2} > \sigma_{ex,1}$ belongs to the higher-energy side. In case of the 3D perovskite FA_{0.9}Cs_{0.1}PbI₃ this was not needed, so $\sigma_{ex} = \sigma_{ex,1} = \sigma_{ex,2}$. Additionally the 1s excitonic peak will show stronger absorption due to a strong exciton-lattice coupling, which can be captured by an additional dielectric confinement factor Df. More details on these corrections can be found in a recent study.^[S8]

$$\alpha_{ex}(E) = \alpha_{1s}(E) + \alpha_{ms}(E)$$

$$\alpha_{1s}(E) = Df \cdot 4\pi \cdot E_B^{3/2} \cdot \frac{1}{\sqrt{2\pi \cdot \sigma_{ex}^2}} \cdot e^{-\frac{1}{2} \left(\frac{E - (E_g - E_B)}{\sigma_{ex}^2} \right)^2}, \text{ where } \begin{cases} E \leq E_g - E_B, & \sigma = \sigma_{ex1} \\ E > E_g - E_B, & \sigma = \sigma_{ex2} \end{cases}$$

$$\alpha_{ms}(E) = \sum_{m=2}^{11} \frac{4\pi \cdot E_b^{3/2}}{m^3} \cdot \frac{1}{\sqrt{2\pi \cdot \sigma_{ex1}^2}} \cdot e^{-\frac{1}{2} \left(\frac{E - E_{xm}}{\sigma_{ex1}^2} \right)^2}, \text{ where } E_{xm} = \frac{E_g - E_B}{m^2} \quad (\text{S3})$$

To model the continuum of states, a simple square-root function can be used, which will be 0 below the bandgap. It is first enhanced by the Sommerfeld factor (SF), which considers strong coulombic interactions of free carriers in a lattice (SF = $\frac{2\pi \cdot E}{1 - e^{(-2\pi \cdot E)}}$ in **Equation S4**; equals

Equation 3.8 in K. Blum *et. al.* paper).^[S9] To account for energetic disorder near the bandgap, an additional broadening is needed. In this case the square-root function is broadened by an additional normalized gaussian with broadening σ_c .

$$\begin{aligned}
\alpha_c(E) &= (b * \alpha_{c,0}(E)) \\
\alpha_{c,0}(E) &= \frac{2\pi \cdot E}{1 - e^{(-2\pi \cdot E)}} \cdot \sqrt{E - E_g} \quad , \text{where } E > E_g \\
b &= \frac{\frac{1}{\sqrt{2\pi \cdot \sigma_c^2}} \cdot e^{-\frac{1}{2} \left(\frac{E}{\sigma_c}\right)^2}}{\int_0^\infty \frac{1}{\sqrt{2\pi \cdot \sigma_c^2}} \cdot e^{-\frac{1}{2} \left(\frac{E}{\sigma_c}\right)^2} dE} \quad (\text{S4})
\end{aligned}$$

The fitting is done with python using the lmfit package. The convolution of the continuum of states absorption coefficient and its broadening is highly influenced by the fitting range and σ_c . Therefore, both have been fixed and changed manually (+/- 1 meV for FA_{0.9}CS_{0.1}PbI₃ and +/- 10 meV for PEA₂PbI₄, respectively) around the values with the best looking fit. Four fits of the same dataset have been averaged in order to obtain a better estimate for the exciton binding energy. The results are summarized in **Table S1** and shown in **Figure S2**. It is important to understand here that the errors shown in Table S1 describe the spread of the four fit values and are not representative of the actual error of estimation. To overcome the uncertainty of our fitting procedure, we compare the estimated exciton binding energies to literature values. In using PEA₂PbI₄ as a 2D material for this study, we ensure that a wide range of reported methods estimating the exciton binding energy is available to us.

Table S1: Parameters as obtained from four Elliott fits. The errors shown are standard errors between the four fits.

	FA _{0.9} CS _{0.1} PbI ₃	PEA ₂ PbI ₄
A [-]	111 +/- 40	14.47 +/- 0.00
E _B [meV]	7 +/- 3	229 +/- 1
E _g [eV]	1.55 +/- 0.02	2.63 +/- 0.01
$\sigma_{\text{ex},1}$ [meV]	18 +/- 1	18 +/- 1
$\sigma_{\text{ex},2}$ [meV]	-	61 +/- 1
σ_c [meV]	19 +/- 1	100 +/- 10
Df [-]	-	4.47

SI.4 Notes on the fitting of k_1 , k_2 , k_3 and k_{ex} from Time-resolved photoluminescence decays and photoluminescence quantum yield

Free-Carrier Fraction of 2D PEA₂PbI₄

In this section, we want to explain the methodology used to estimate the fraction of free carriers by knowledge of the exciton binding energy E_B as well as the recombination constants k_1 , k_{ex} , k_2 and k_3 .

The fraction of free carriers in an equilibrium situation can be estimated from the Saha equation (Equation (3) from the main text):^[S10]

$$\frac{\phi^2}{1-\phi} = \frac{1}{N} \cdot \left(\frac{2\pi \cdot \mu_0 \cdot k_B T}{h^2} \right)^{3/2} \cdot e^{-\frac{E_B}{k_B T}} \quad (\text{S5})$$

It has been shown in recent work that this relation also holds true for 2D Ruddlesden-Popper perovskites, which show highly excitonic behaviour.^[S11,S12] In their work a full kinetic model is derived to describe the interplay of excitons and free carriers. The free carrier ratio as determined from the Saha equation (**Equation S5**) is then compared to the ratio as estimated from the exciton dissociation rate and free-carrier recombination rate. In the case where emission only occurs from the excitonic state and not from free carriers, both methods should yield the same result. The work reports this for $n = 1$ PEA₂PbI₄.

This result suggests that the photoluminescence intensity $I(n)_{t=0}$ (or PL₀) will scale linearly with n in case of the excitonic, 2D material. In **Figure S3** the PL₀ (measured with TPC pulsed laser and PMT detector) is shown for different carrier densities as calculated from laser fluences and thin-film absorption. Both PEA₂PbI₄ and FA_{0.9}Cs_{0.1}PbI₃ are shown. Clearly, for PEA₂PbI₄ there is a linear relation ($b = 1$):

$$PL_0 \sim n^b \quad (\text{S6})$$

It is worth mentioning that this relation is currently under active debate as $b > 1$ behaviour has been observed in 2D perovskites as well.^[S13,S14] The explanation brought forward is polaron formation as well as fast initial annihilation of a minority of excitons. For our work, the exact mechanism of this is less important, since $b = 1$ behaviour is observed and the transient photoconductivity (TPC) as well as terahertz spectroscopy (OTTP) can only probe the free-carrier mobility.

Much more important however, is the change of PL after pulsed excitation, which can be described with the commonly known relation (Equation 4 in the main text), including the non-radiative trap-assisted recombination (k_1) and Auger recombination (k_3) as well as radiative recombination and exciton recombination (k_2 and k_{ex}). In the study mentioned above k_{ex} was related to k_2 -like recombination via the free carrier density in equilibrium (n_{eq}).^[14] This one is directly linked to the Saha equilibrium (**Equation S5**) via:

$$n_{eq} = \frac{n_{free}^2}{n_{ex}} = \frac{\phi^2}{1-\phi} \cdot N_{tot} \quad (\text{S7})$$

where N_{tot} is the total carrier density as calculated from the laser fluence and thin film absorption, n_{free} is the free-carrier density, n_{ex} the exciton density. It becomes apparent that the influence of $\frac{k_{ex}}{n_{eq}}$ on $k_{2,eff}$ will be negligible for a 3D perovskite (like FA_{0.9}Cs_{0.1}PbI₃), since $\phi \sim 1$ and hence $n_{eq} \sim N_{tot}$. However for an excitonic material like PEA₂PbI₄ this additional dynamic, namely the dissociation of excitons into free carriers and its reverse reaction, needs to be included. Additionally, under the fluences probed the carrier density is not high enough to reach significant levels of k_3 recombination and can be neglected as well.

One can then simplify Equation 4 from the main text to:

$$-\frac{dn}{dt} = k_1 n + \left(k_2 + \frac{k_{ex}}{n_{eq}}\right) n^2 = k_1 n + k_{2,eff} n^2 \quad (\text{S8})$$

where $k_{2,eff}$ now includes the monomolecular, radiative exciton recombination k_{ex} and the equilibrium carrier concentration defined via:

To be able to use **Equation S7** for the global fitting of TRPL transients, one needs to integrate it. Here we use the solution derived by B. Ohnesorge *et. al.*, as well as **Equation S6** for $b = 1$ to obtain:^[S15]

$$PL_{norm}(t) = B \cdot k_1 \cdot \frac{e^{-k_1 t}}{1 + \left(\frac{k_{2,eff}}{k_1}\right) \cdot n_{tot} \cdot (1 - e^{-k_1 t})} \quad (\text{S9})$$

where B is an instrument-specific scaling parameter. From a global fit of the TRPL transients for different n_{tot} , k_1 can be estimated with high accuracy. A value for $k_{2,eff}$ can be obtained, but it is not very meaningful here, because its processes are too fast to be fully captured by the TRPL transients. Instead, intensity-dependent PLQE using a continuous light source can be used. The PLQE can be estimated from the recombination constants as:

$$PLQE = A \cdot \frac{k_{2,eff} n}{k_1 + k_{2,eff} n + k_3 n^2} \xrightarrow{n = n_{eq}} A \cdot \frac{k_{ex} + k_2 n_{eq}}{k_1 + k_{ex} + k_2 n_{eq} + k_3 n_{eq}^2} \quad (\text{S10})$$

where A is an instrument-specific scaling parameter and the right-hand side corresponds to Equation (5) in the main text as also previously reported for 2D systems.^[S16]

It is needed in this case to be able to fit the intensity-dependent PLQE of PEA_2PbI_4 , which almost unchanged over a wide range of carrier densities, but only at $\sim 1\%$.

It is worth mentioning at this point that there is generally a large error associated with PLQE measurements. We try to overcome this error, by measuring several spots across several samples for each material and fluence (in total 9 spots across 3-4 samples, typically). This also allows us to measure low PLQE values at lower fluences, even though the data itself is much noisier. We show a representative set of PL spectra comparing the lowest and highest fluences measured for both PEA_2PbI_4 and $\text{FA}_{0.9}\text{Cs}_{0.1}\text{PbI}_3$ in Figure S.5. Clearly, the low-fluence data has a higher uncertainty, but after measuring several spots this will be captured in the standard error as shown in the main text in Figure 2. We ascribe the larger error bars of the $\text{FA}_{0.9}\text{Cs}_{0.1}\text{PbI}_3$ data to a larger sample-to-sample variation.

Fitting Procedure for k_1 , k_{ex} , k_2 and k_3

To obtain the recombination constants time-resolve PL transients are first normalized and then the background value (before the pulse at $t = 0$) is subtracted from the data. Via this processing, only real decay phenomena will be observable. Three different fluences are probed and a global fit of **Equation S7** starting 150 ns (20 ns for FA_{0.9}CS_{0.1}PbI₃) after the pulse is used to estimate k_1 . The reasoning for this is shown in **Figure S4**, where the same set of data is presented in two different ways (dn/dt vs. n and n vs time). It can be clearly seen that the decay is only dominated by k_1 , after a certain carrier density is reached and that this happens after 150 ns (20 ns) for all three fluences. The obtained k_1 values are summarized in Table 1 in the main text.

Next, the intensity dependent PLQE was measured using 4 films and 3 spots on each film. From the laser fluence and thin film absorption a generation rate G can be estimated for the continuous illumination. In steady state $dn/dt = 0$ and one can solve

$$G = k_1 n_{ss} + k_2 n_{ss}^2 + k_3 n_{ss}^3 \quad (\text{S11})$$

to obtain n_{ss} as the carrier density in the steady-state condition. We make the assumption here that n_{ss} will be close to n_{eq} and can be used to solve **Equation S10**. The tricky part is that initial guess parameters for k_2 and k_3 are needed to obtain n_{ss} . The initial guesses were taken from G. Xing. et. al. and the PLQE was fitted using **Equation S10**.^[S16] Then **Equation S11** was solved again with the new parameters. These two steps were repeated until a good agreement between literature and data was obtained. The extracted parameters can be found in **Table 1** in the main text. In all cases the instrument-specific parameter A was fitted as 1.8.

SI.5 Fitting and Correcting the TPC and THzC Data

The transient photoconductivity is measured in a home-built setup that monitors the change in electric current under illumination as a voltage change in an oscilloscope (see our recent report on a much more detailed description of the method).^[S1] The conductivity is calculated from that and then the mobility can then be extracted via Equation 2 in the main text:

$$\sigma_{t=0} = \mu \cdot N_0\phi \cdot e \quad (\text{S12})$$

To obtain $\sigma_{t=0}$ a biexponential decay is fitted to the traces with the fitting range starting 100-150 ns after the pulse trigger. The traces for each laser fluence measured are fitted separately. One representative set of data with the biexponential fits overlaid is shown in **Figure S6**. The sum mobility is highly dependent on the accurate estimations of $N_0\phi$, which is corrected after the measurement. During the laser pulse, local carrier concentrations might get higher and access different recombination mechanisms, which will reduce the free carrier ratio. At the same time the equilibrium free carrier ratio is determined by the Saha equation (**Equation S5**), which predicts an increasing ratio ϕ , because the carrier density n is decaying over time. The estimated exciton binding energy and recombination constants are therefore needed to find the free carrier ratio at $t = 0$.

First, **Equation S13** is solved using a python script. To estimate the generation rate G , the excitation density is broadened by a gaussian with a full-width at half maximum (fwhm) of 3.74 ns (the pulse-width of the laser used).^[S1]

$$\frac{dn}{dt} = G - k_1n - k_2n^2 - k_3n^3, \text{ where } G = n_{tot} * gauss \quad (\text{S13})$$

This will yield the decay of carriers generated by the laser pulse and cannot be resolved with the setup, due to the long laser pulse-width (low early-time resolution). Each calculated carrier density is then corrected by the Saha equilibrium (**Equation S5**) to yield a time-resolved free-carrier ratio. Its maximum value appears a few ns after the initial pulse and is assumed to be closest to the initial equilibrium free-carrier concentration. It is called the free carrier density at t_{max} and is used in place of $N_0\phi$, to calculate the true sum-mobility.

SI.6 Error Estimation for TPC Corrections

After making a few assumptions and estimating different parameters, it is necessary to estimate the error that can be made by these corrections. We show it here for PEA_2PbI_4 , but a similar analysis has been done for three-dimensional perovskites in our recent study.^[S1] The calculations described in SI.5 were repeated, but each parameter (E_B , k_1 , k_2 and k_3) was varied according to the error that could potentially be made: k_1 & k_2 +/- one order of magnitude, k_3 +/- one or two orders of magnitude and E_B +/- 1 or 10 meV. The resulting data are plotted in **Figure S7A**. In case of k_1 , only an overestimation would have a noticeable impact on the resulting mobility. This is in line with a higher k_1 corresponding to shorter lifetimes, which may then influence the early-time recombination dynamics as well. Similarly, k_2 and k_3 only show a change in mobility, if the error is an overestimation, leading to faster decays in all cases. Interestingly, an error in k_1 will mainly affect the mobility estimated at lower carrier densities, while k_2 and k_3 affect the mobility estimated under higher excitation fluences, which can be understood by their order in **Equation S13** or Equation 4 in the main text. In contrast to these changes, an error in E_B will not dramatically affect the shape of the carrier-density-dependent mobility, but rather just shift it to higher/lower carrier densities in accordance with **Equation S5**, and shift the absolute values of mobility up and down. Next, we try to understand, which of these errors have the most impact, and the scale of impact upon the estimated mobility. For that we calculate the average of a single set of data (over 4 different intensities, black curve in **Figure S7A**) and estimate the corresponding mobility values for a range of changes in the relevant parameters. We thus estimate a “relative error” in the calculated mobility, for a corresponding uncertainty in any of the key parameters. We compare these errors to the relative statistical error from multiple measurements. The resulting relative errors are shown in **Figure S7B**. A few things become apparent from this analysis: The statistical error (standard deviation) within a single set of data is relatively small at around +/- 5%. The error introduced by varying k_1 by one order of magnitude is around 8%. 2) k_2 and k_3 need a good estimate, but as discussed previously, they can be underestimated, but not overestimated. As long as k_2 and k_3 are not overestimated the relative error in mobility is still below 10%. If our estimation of E_b is accurate to within 1meV, then its impact upon the error is below 5%. If E_b is accurate to within 10meV, possibly the most likely scenario, then its impact upon the error is dominating, at around 20%. However, since charge carrier mobility is a value that can vary by many orders of magnitude, the relative impact of errors in these estimated parameters upon the calculated value of the charge carrier mobility is relatively low. Finally, the experimental parameters used to acquire all the data used in this study (of PEA_2PbI_4) are summarized in **Table S2** and the corresponding calculated mobilities are collectively plotted in **Figure S7C**.

Table S2: Summary of batches used for this project for PEA₂PbI₄. The number of scans per device were performed on the same spot, just a few seconds after the first set. The thickness was determined using a DekTak Profilometer. During the measurement the laser intensity is changed from a high OD filter to a lower one in 0.5 steps.

	#Devices (Scans)	Thickness [nm]	Electric Field [V μm^{-1}]	Laser Wavelength [nm]	Laser Power Density [W cm^{-2}]	OD Filters (in 0.5 steps)
A	4 (3)	270 +/- 48	0.011	470	0.0095	1.0 - 3.5
B	4 (2) ^a	155 +/- 16	0.009	450	0.0026	1.0 - 3.5
C	2 (2)	383 +/- 38	0.005	450	0.0043	1.5 - 4.0
C*	1 (2)	383 +/- 38	0.005	470	0.0080	1.5 - 4.0
D	4 (2)	592 +/- 72	0.009	470	0.0080	2.5 - 5.0
E	3 (2)	386 +/- 27	0.009	470	0.0080	2.0 - 4.0
F	1 (2)	359 +/- 52	0.009	470	0.0080	1.5 - 4.0

^a half of the samples made from single crystal precursors

SI.7 Extracting Mobility from the OPTP Experiments

The effective charge-carrier mobility was extracted from the amplitude of the OPTP signal immediately after photoexcitation (i.e. before charge-carrier recombination occurs). The sheet photo-conductivity, ΔS , of a material with a thickness much shorter than the wavelength of the THz radiation can be expressed as

$$\Delta S = -\epsilon_0 c (n_a + n_b) (\Delta T / T) \quad (\text{S14})$$

where n_a and n_b are the THz refractive indices of the materials interfacing the perovskite layer at the front and rear respectively. The quantity $\Delta T / T$ is the ratio of the photo-induced change in THz electric field to the transmitted THz electric field in the dark. The initial number of photo-excited charge carriers N is given by

$$N = \varphi \frac{E\lambda}{hc} (1 - T_{pump} - R_{pump}) \quad (\text{S15})$$

with E being incident pump pulse energy, λ the excitation wavelength, φ the ratio of free charges created per photon absorbed, and R_{pump} and T_{pump} being the reflected and transmitted fractions of the pump beam intensity. These two equations can be used to extract the charge-carrier mobility μ through

$$\mu = \frac{\Delta S A_{eff}}{Ne} \quad (\text{S16})$$

where A_{eff} is the effective area from the overlap of the pump and probe beams and e is the elementary charge. Substituting Equations S1 and S2 into Equation S3 we obtain

$$\varphi \mu = -\frac{\epsilon_0 c (n_a + n_b) (A_{eff})}{Ne \lambda (1 - R_{pump}) (1 - T_{pump})} \left(\frac{\Delta T}{T} \right) \quad (\text{S17})$$

from which the effective charge-carrier mobility $\varphi \mu$ may be determined based on the pump beam parameters and the initial measured $\Delta T / T$ of the sample. Here, μ is the charge-carrier mobility, and φ is the charge-to-photon branching ration which is assumed to be unity at room temperature.

SI.8 Comments on the use of the Saha equation

The Saha equation (equation 3 in the main text) can be used to estimate the free-carrier fraction based on the exciton binding energy of a material and the excitation density (cm^{-3}). It is a good estimate for three-dimensional semiconductors, where the generated charge carriers can quickly diffuse throughout the whole layer thickness.

However, for two-dimensional materials, the anisotropy of charge carrier transport complicates its use. In general, a version of the Saha equation exists for 2D materials, taking this into account, by estimating a fluence per quantum well thickness (N ; $\text{cm}^{-2} \text{ well}^{-1}$) instead of the excitation density. The equation then is:

$$N_{2D} \cdot \frac{\phi^2}{1-\phi} = d \cdot \frac{2\pi \cdot \mu_0 \cdot k_B T}{h^2} \cdot e^{-\frac{E_B}{k_B T}} \quad (\text{S18})$$

where d is the thickness of the quantum well and not the layer thickness of the thinfilm. In

Figure S18 we compare the two versions of the Saha equation for PEA_2PbI_4 and find a good agreement for $d = 15 \text{ nm}$. For better comparability with $\text{FA}_{0.9}\text{Cs}_{0.1}\text{PbI}_3$ we hence use the '3D'-version of the Saha equation (Equation 3) as shown in the main text.

Supplementary References

- [S1] J. Lim, M. Kober-Czerny, Y.-H. Lin, J. M. Ball, N. Sakai, E. A. Duijnste, M. J. Hong, J. G. Labram, B. Wenger, H. J. Snaith, *Nat. Comms.* 2022, under submission.
- [S2] C. Wehrenfennig, M. Liu, H. J. Snaith, M. B. Johnston, L. M. Herz, *Energ Environ Sci* 2014, 7, 2269.
- [S3] C. Wehrenfennig, G. E. Eperon, M. B. Johnston, H. J. Snaith, L. M. Herz, *Adv Mater* 2014, 26, 1584.
- [S4] J. C. de Mello, H. F. Wittmann, R. H. Friend, *Adv Mater* 1997, 9, 230.
- [S5] R. J. Elliott, *Phys Rev* 1957, 108, 1384.
- [S6] C. L. Davies, M. R. Filip, J. B. Patel, T. W. Crothers, C. Verdi, A. D. Wright, R. L. Milot, F. Giustino, M. B. Johnston, L. M. Herz, *Nat Commun* 2018, 9, 293.
- [S7] J. V. Passarelli, C. M. Mauck, S. W. Winslow, C. F. Perkinson, J. C. Bard, H. Sai, K. W. Williams, A. Narayanan, D. J. Fairfield, M. P. Hendricks, W. A. Tisdale, S. I. Stupp, *Nat Chem* 2020, 12, 672.
- [S8] S. Neutzner, F. Thouin, D. Cortecchia, A. Petrozza, C. Silva, A. Ram, S. Kandada, *Phys Rev Mater* 2018, 2, 64605.
- [S9] M. Cirelli, T. Hambye, P. Panci, al -, M. Aoki, T. Toma, A. V. -, J. Chen, Z.-L. Liang, Y.-L. Wu, *J Cosmol Astropart P* 2016, 2016, 021.
- [S10] M. N. Saha, *Proc. R. Soc. Lond. Series A* 1921, 99, 135.
- [S11] A. A. Burgos-Caminal, E. Socie, M. E. F. Bouduban, J.-E. Moser, *J Phys Chem Lett* 2020, 11, 18.
- [S12] N. Spitha, D. D. Kohler, M. P. Hautzinger, J. Li, S. Jin, J. C. Wright, *J Phys Chem C* 2020, 124, 41.
- [S13] W. Wang, Y. Li, X. Wang, Y. Liu, Y. Lv, S. Wang, K. Wang, Y. Shi, L. Xiao, Z. Chen, Q. Gong, *Sci Rep-uk* 2017, 7, 14760.
- [S14] A. Simbula, R. Pau, Q. Wang, F. Liu, V. Sarritzu, S. Lai, M. Lodde, F. Mattana, G. Mula, A. G. Lehmann, I. D. Spanopoulos, M. G. Kanatzidis, D. Marongiu, F. Quochi, M. Saba, A. Mura, G. Bongiovanni, *Adv Opt Mater* 2021, 9, 2100295.
- [S15] B. Ohnesorge, R. Weigand, G. Bacher, A. Forchel, W. Riedl, F. H. Karg, *Appl Phys Lett* 1998, 73, 1224.
- [S16] G. Xing, B. Wu, X. Wu, M. Li, B. Du, Q. Wei, J. Guo, E. K. L. Yeow, T. C. Sum, W. Huang, *Nat Commun* 2017, 8, 14558.

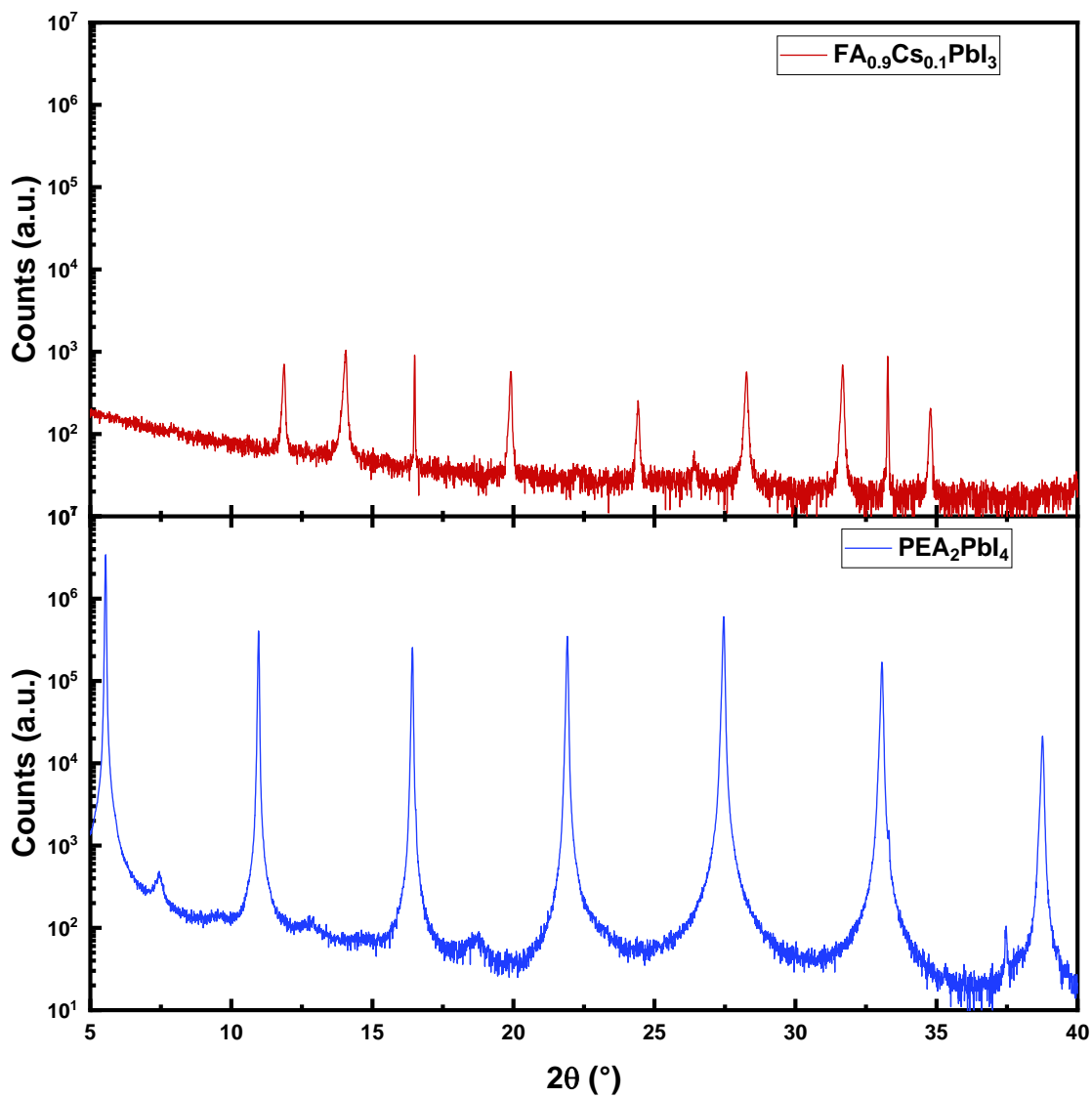


Figure S1. 1D XRD patterns of the 3D (top) and 2D (bottom) perovskite assessed in this study. Both were measured on z-cut quartz substrates.

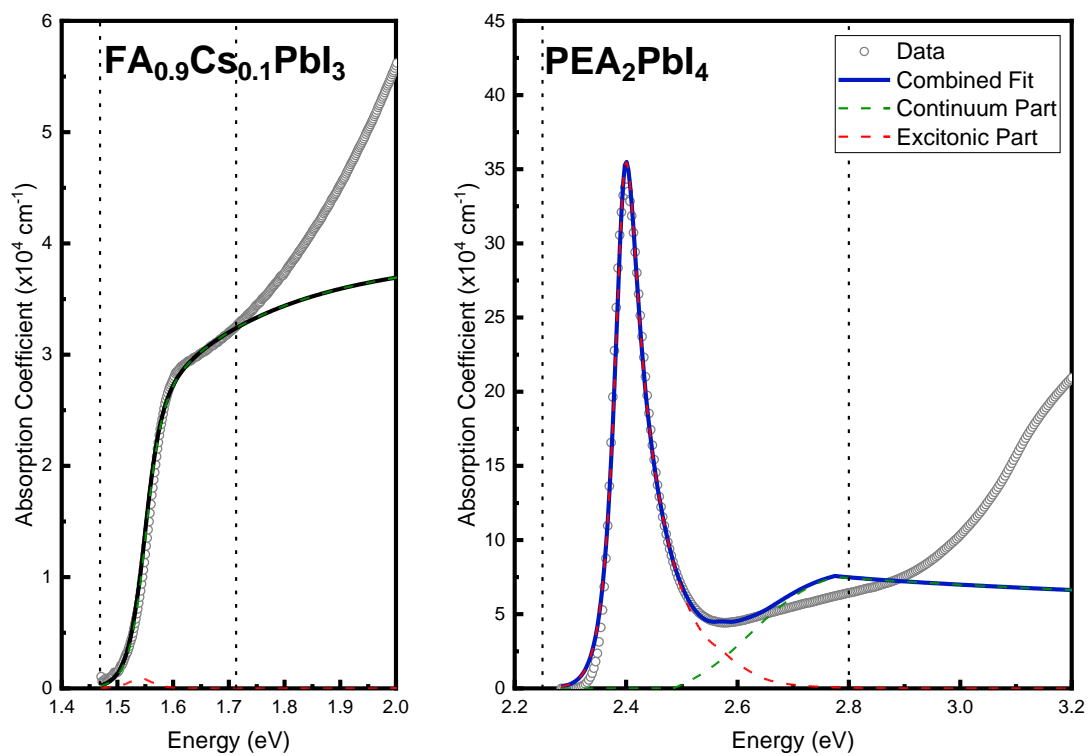


Figure S2. The absorption coefficient for both $\text{FA}_{0.9}\text{Cs}_{0.1}\text{PbI}_3$ and PEA_2PbI_4 are shown. For both sets of data the Elliott Fit was done and its excitonic and continuum part are presented as well as the resulting sum of both parts. The straight dotted lines represent the fitting limits.

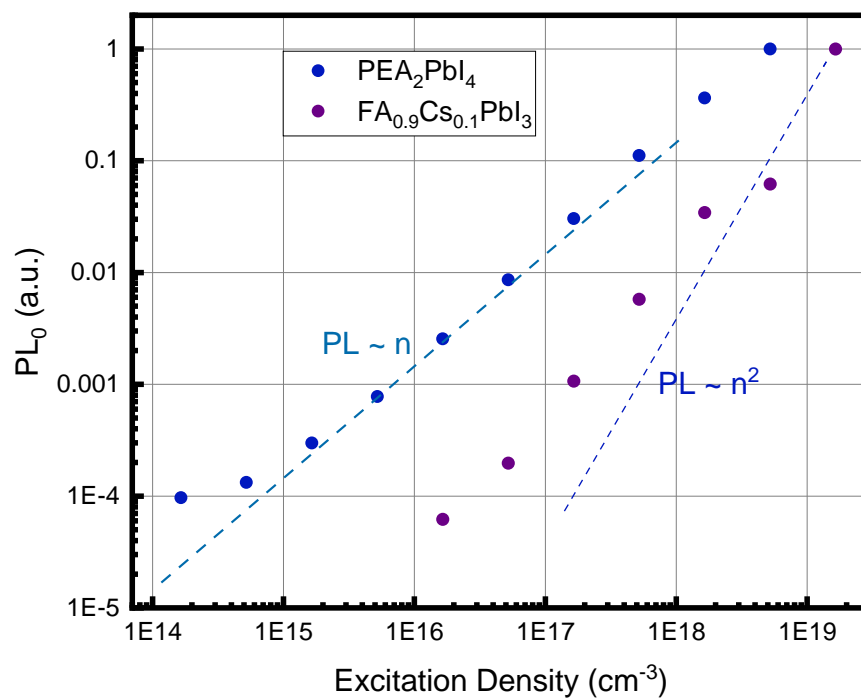


Figure S3. The initial PL intensity (PL_0) is presented as a function of excitation density as calculated from the laser fluence and film absorption properties. The lines following the $PL \sim n$ as well as $PL \sim n^2$ are plotted with the data as a guide to the eye.

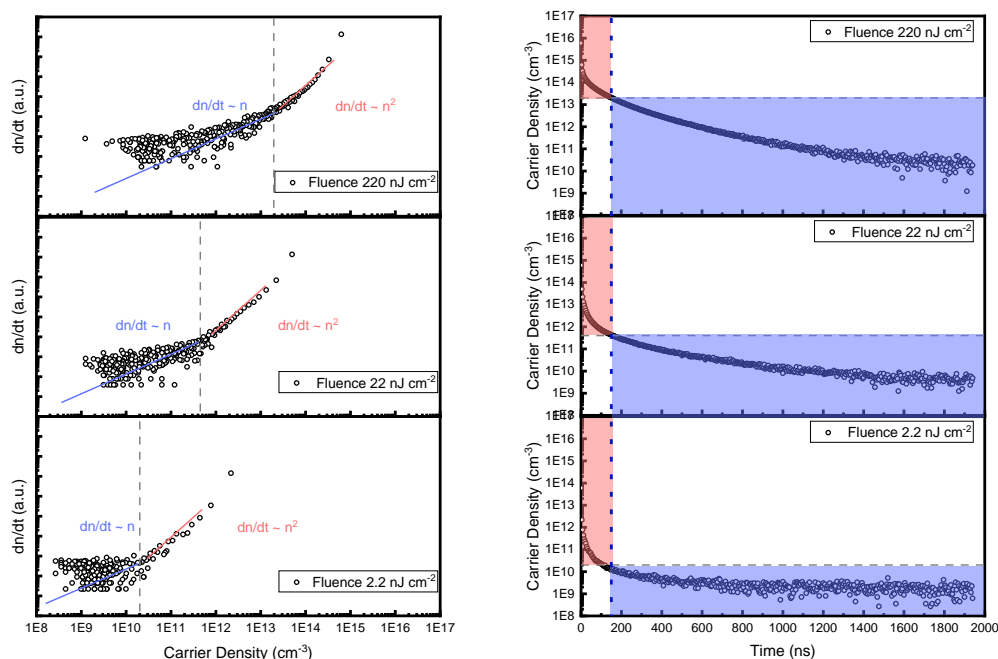
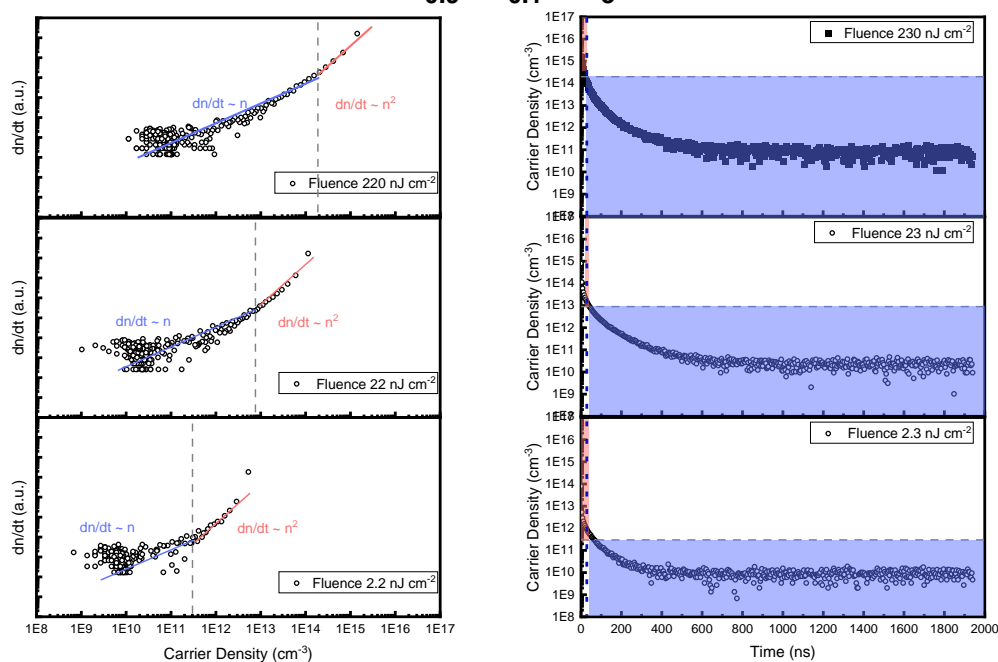
PEA₂PbI₄FA_{0.9}Cs_{0.1}PbI₃

Figure S4. One set of TRPL transients for all three fluences are shown for PEA₂PbI₄ (Top) and FA_{0.9}Cs_{0.1}PbI₃ (Bottom) in two different presentations: (Right): the normalized data has been multiplied by the excitation density as calculated from the laser fluence and the film absorption properties, then dn/dt was calculated as $(n_t - n_{t+1})/4 \text{ ns}$. The blue and red line are guides to the eye to determine the point at which the k_2 -dominated decay ($dn/dt \sim n^2$) changes to a k_1 -dominated one ($dn/dt \sim n$). (Right): The data is presented as the normal decay scaled by the excitation density.

The red regions are k_2 -dominated decays, while the blue are k_1 -dominated, as determined from the point of change in the left plots.

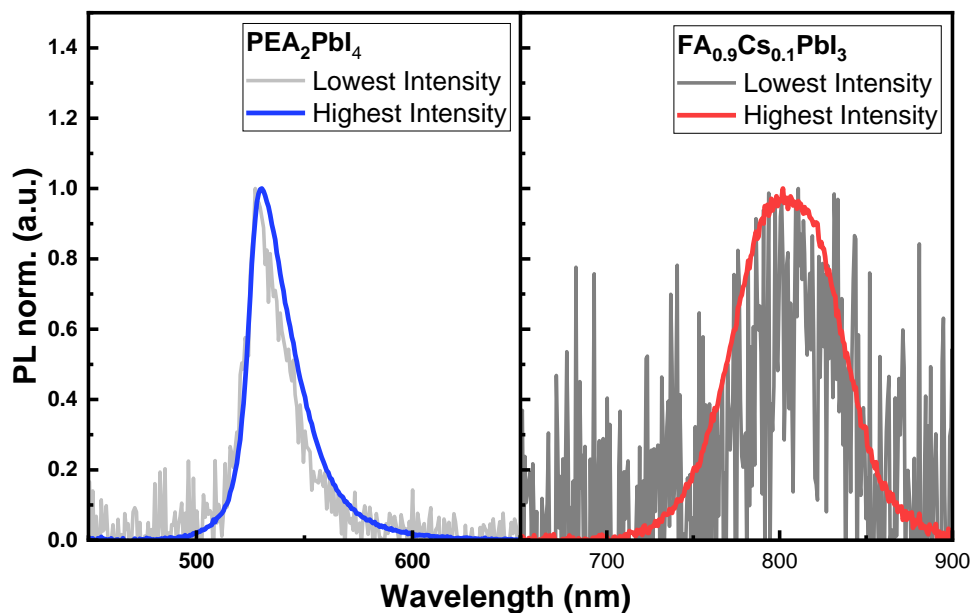


Figure S5. Representative PL traces for PEA_2PbI_4 and $\text{FA}_{0.9}\text{Cs}_{0.1}\text{PbI}_3$ as obtained from the PLQE measurements for the lowest and highest laser intensities used in each set of measurements.

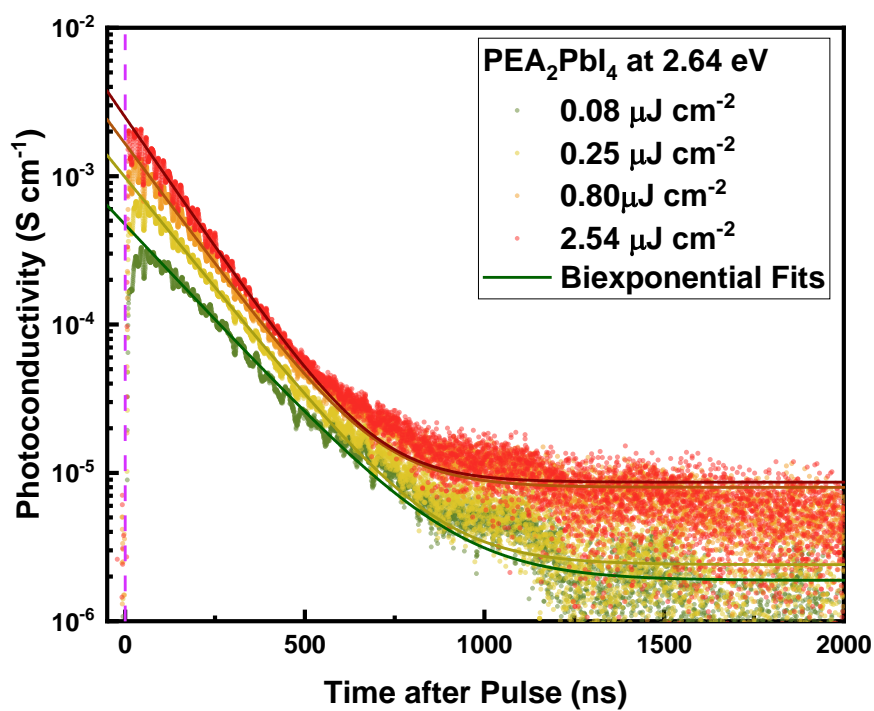


Figure S6. Representative TPC traces for PEA₂PbI₄ with the biexponential fits used to obtain $\sigma_{t=0}$ ($t = 0$ is shown as pink dashed line). The fitting range was 100-2000 ns after the pulse.

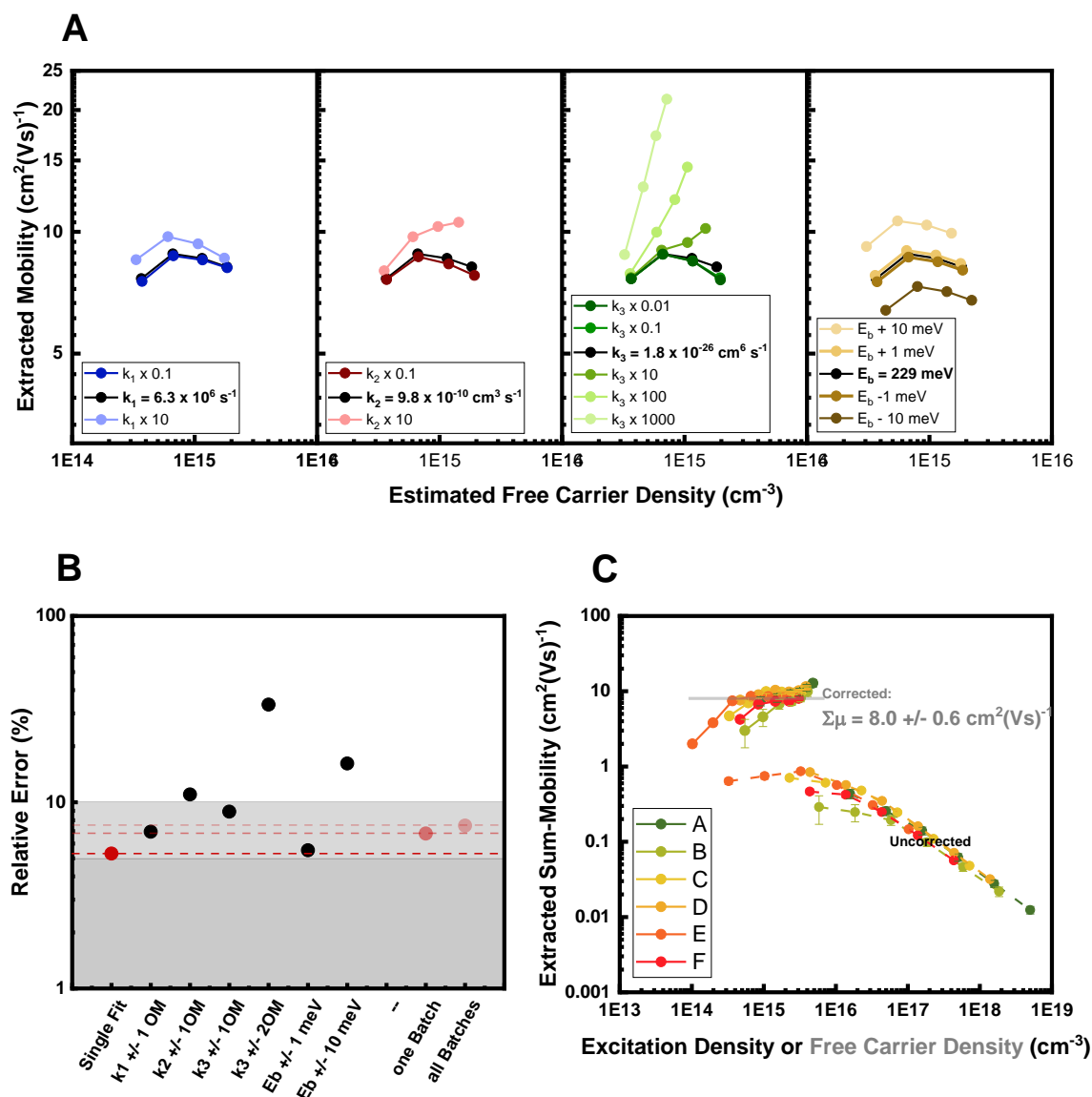


Figure S7. A: Error estimation for the TPC corrections of PEA_2PbI_4 . Each parameter is changed with respect to the best estimates summarized in Table S1. The processed data using $k_1 = 6.3 \times 10^6 \text{ s}^{-1}$ and $k_1 \times 0.1$ overlap almost perfectly. B: The data in A are averaged over all carrier densities, and the relative error in the sum of the charge carrier mobilities is calculated (for example $k_1 \pm 1 \text{ OM}$ means range of estimated mobility, using the range of k_1). The red data points with corresponding lines show the errors estimated by a single fit, three films within one batch and all batches, as summarized in Table S2. The dark and light grey areas represent the 5% and 10% relative error regions respectively. C: Summarised mobility data of all the PEA_2PbI_4 batches used in this project (as shown in Table S2). The uncorrected as well as corrected data are presented side-by-side.

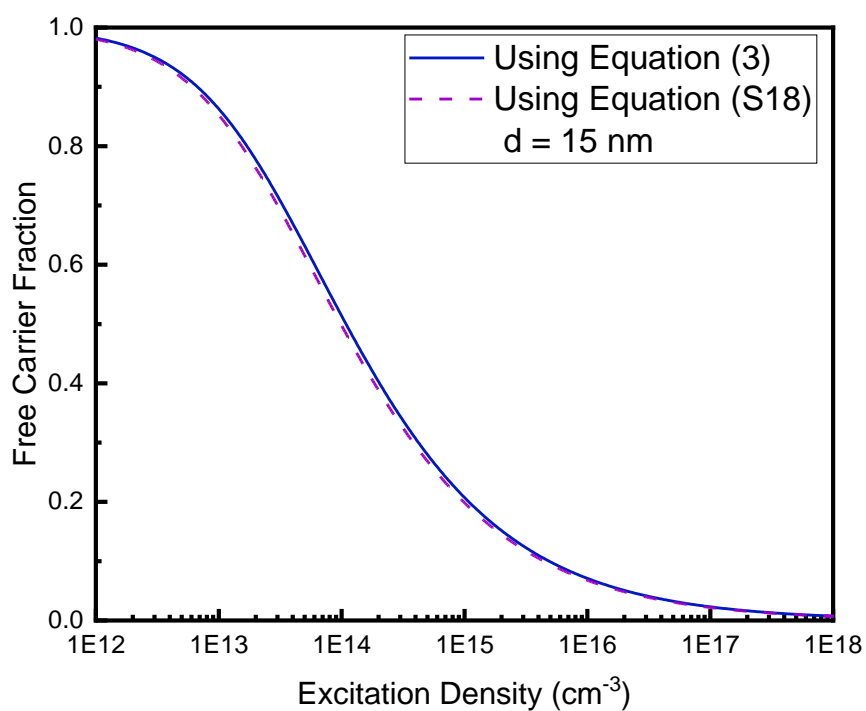


Figure S8. Estimation of the free-carrier fraction of PEA_2PbI_4 ($E_B \sim 229$ meV) using the 3D-Saha equation (Equation 3 in the main text) and the 2D-Saha equation (Equation S18) for the relevant excitation densities in this study.